Nano Energy 89 (2021) 106363

Contents lists available at ScienceDirect

Nano Energy

journal homepage: www.elsevier.com/locate/nanoen

Communication

# All-inorganic triboelectric nanogenerators based on $Mo_6S_3I_6$ and indium tin oxide☆

Renyun Zhang [a,*], Magnus Hummelgård [a], Jonas Örtegren [a], Martin Olsen [a], Henrik Andersson [b], Ya Yang [a,c,d,e], Zhong-Lin Wang [c,f], Håkan Olin [a], Petra Sutar [f], Dragan Mihailovic [f,*]

[a] Department of Natural Sciences, Mid Sweden University, Holmgatan 10, SE85170 Sundsvall, Sweden
[b] Department of Electronics Design, Mid Sweden University, Holmgatan 10, SE85170 Sundsvall, Sweden
[c] CAS Center for Excellence in Nanoscience, Beijing Key Laboratory of Micro-nano Energy and Sensor, Beijing Institute of Nanoenergy and Nanosystems, Chinese Academy of Sciences, Beijing 101400, PR China
[d] School of Materials Science and Engineering, Georgia Institute of Technology, Atlanta, GA 30332-0245, USA
[e] Beijing Institute of Nanoenergy and Nanosystems, Chinese Academy of Sciences, Beijing 101400, PR China
[f] Jozef Stefan Institute, Faculty of Mathemics and Physics, University of Lj ubljana, Jadranska 19, Ljubljana, Slovenia CENN Nanocenter, Jamova 39, 1000 Ljubljana, Slovenia

ARTICLE INFO

*Keywords:*
Inorganic materials
Triboelectric nanogenerators
$Mo_6S_3I_6$
Indium tin oxide

ABSTRACT

Triboelectrification can occur between any two materials with different charge affinities. This phenomenon represents the fundamental physics of triboelectric nanogenerators (TENGs). Organic materials such as polymers have been widely used in TENGs because of their dielectric properties. Inorganic materials are, however, not widely studied despite the increasing attention paid to perovskite materials. In this paper, a new type of TENG has been fabricated based only on inorganic materials such as $Mo_6S_3I_6$ and indium tin oxide (ITO). The output power density of the TENG operating in contact-separation mode reaches 18 W $m^{-2}$. Mechanisms of the high output involve the unique semiconducting property of $Mo_6S_3I_6$ and the unique chemical composition of ITO. The findings in this study indicate that inorganic materials can be used for fabricating high-output TENGs for energy harvesting.

## 1. Introduction

Materials for TENGs [1] are very diverse and include polymers,[2–4] metals,[5,6] semiconductors [7,8] and nonmetal inorganic materials. [9] Polymers such as PTFE, [10–12] FEP, [13–15] PI, [13,16,17] PDMS, [18–20] and PET [21–23] are most frequently utilized triboelectric materials due to their excellent triboelectric effects and unique physical properties, such as elasticity. Metals are commonly used as both triboelectric materials for generating triboelectric charges and electrodes for conducting electrons. Semiconductors, especially two-dimensional ones such as $MoS_2$ and $WS_2$, [7,8] have also gained much interest because their semiconducting properties may bring more features to TENGs. Zou and coworkers [24] recently characterized the triboelectric effects of different nonmetallic materials, such as mica, glass, and boron nitride, showing the connections between the triboelectric charge densities and the work functions of the materials.

Inorganic materials, except those metals mentioned above, are not as widely used in TENGs as organic materials because of their low output and the difficulties of making thin films for constructing TENGs. On the other hand, the thermal stability and resistance to irradiation make inorganic materials attractive for constructing TENGs. Recently, inorganic perovskite materials such as $CsPbX_3$ [9] have been used for making TENGs, and the output power has been found to be approximately 1.2 W $m^{-2}$. Perovskite nanoarrays [25] of rhombus $Co(OH)(CO_3)_0.5$/Pt/$CsPbIBr_2$ boost charge transfer and increase the output power density to 2.04 W $m^{-2}$. New types of alloys, such as silicon-alloyed aluminum substrates, [26] have also been used in TENGs and exhibit an output power density of approximately 11.2 W $m^{-2}$.

Despite the increasing interest in applying inorganic materials in TENGs, the choice of inorganic materials is still limited. New materials

☆ Prof Zhong Lin Wang, an author on this paper, is the Editor-in-Chief of Nano Energy, but he had no involvement in the peer review process used to assess this work submitted to Nano Energy. This paper was assessed, and the corresponding peer review managed by Professor Chenguo Hu, an Associate Editor in Nano Energy

* Corresponding authors.
*E-mail addresses:* renyun.zhang@miun.se (R. Zhang), dragan.mihailovic@ijs.si (D. Mihailovic).

https://doi.org/10.1016/j.nanoen.2021.106363
Received 12 June 2021; Received in revised form 8 July 2021; Accepted 19 July 2021
Available online 22 July 2021

with good triboelectric effects are in high demand for extending the application of TENGs. One candidate could be $Mo_6S_3I_6$, a one-dimensional van der Waals material [27,28] in which small-diameter nanowires are weakly bound in bundles by van der Waals forces. [29] $Mo_6S_3I_6$ is a quasi-one-dimensional conductor [30] when the nanowires are well bundled. However, the unbundled nanowires that have been found are semiconducting [31] with a bandgap of 1.2–1.5 eV and a work function of 4.78 eV. The material has been observed to respond strongly to an electrostatic field, making it an attractive material for use in TENGs.

In this paper, we report an all-inorganic material-based TENG fabricated with $Mo_6S_3I_6$ and ITO. The power density of the TENG reaches 18 W $m^{-2}$, which is approximately 10 times higher than those of the other nonmetallic inorganic material-based TENGs. Mechanisms behind the high output include the unique semiconducting property of $Mo_6S_3I_6$ and the specific chemical composition of ITO.

## 2. Results and discussion

### 2.1. Triboelectric effect of $Mo_6S_3I_6$ and ITO

The structure of $Mo_6S_3I_6$ nanowires is shown in Fig. 1(a), which shows a polymer-like structure. Fig. 1(b) and (c) show scanning electron microscopy (SEM) images of $Mo_6S_3I_6$ bundles and $Mo_6S_3I_6$ film on copper tape, and the images were obtained before triboelectric studies. The diameters of the $Mo_6S_3I_6$ bundles were approximately 200 nm [32], and the lengths were in the range of several to tens of micrometers. Fig. 1 (d) shows an SEM image of the film after several contact-separation cycles against ITO (Fig. 1e), indicating that the bundles were destroyed and unbundled nanowires resulted. This unbundling process enhanced the semiconducting behavior of the $Mo_6S_3I_6$ film, leading to the high output of the TENG. The mechanisms for this are discussed in detail below.

The triboelectric effects of $Mo_6S_3I_6$ bundles and ITO have not been well studied before. Therefore, it is important for us to characterize the triboelectric effects for further studies of TENGs constructed with the $Mo_6S_3I_6$/ITO material pair. In this study, the triboelectric effect was investigated by measuring the open-circuit voltage and short circuit current of the triboelectrification between the $Mo_6S_3I_6$ bundles or ITO and different materials (Fig. S1 shows the circuit used for the measurement). After understanding the triboelectric effect of $Mo_6S_3I_6$, we further studied an all-inorganic TENG with the operation mode shown in Fig. 1(f).

We selected different materials, including both organic and inorganic materials, to study the triboelectric effect of $Mo_6S_3I_6$ and ITO. Fig. 2(a) shows the open-circuit voltages between $Mo_6S_3I_6$ and the counter materials. The results indicated that $Mo_6S_3I_6$ can either donate or accept electrons from other materials. The most significant negative open-circuit voltages were found between $Mo_6S_3I_6$ and PTFE, and the most significant positive open-circuit voltage was found between $Mo_6S_3I_6$ and clear cellulose (cellulose acetate). The results also show that the charge affinity of $Mo_6S_3I_6$ is close to those of PI, bentonite and copper, as indicated by the small open-circuit voltages.

The order of the short-circuit currents (Fig. 2b) measured did not follow the same order as the open-circuit voltages. The highest negative current was found between $Mo_6S_3I_6$ and the PFA film, and the highest positive current was measured between $Mo_6S_3I_6$ and the nylon film. The difference between the orders could be due to the differences in thicknesses and dielectric properties of the materials.

Unlike $Mo_6S_3I_6$, ITO has shown stronger positive charge affinity, since it donated electrons to most of the materials that were tested (Fig. 2c). It could only accept electrons from PEI, clear cellulose, nylon and PET. This behavior was consistent with the results shown in Fig. 2 (a), where the ITO was positioned above only these four materials. The highest negative current (Fig. 2d) was measured for the ITO/PFA TENG, and the highest positive current was found for the ITO/PET TENG.

### 2.2. $Mo_6S_3I_6$/ITO based TENG

Characterization of the triboelectric effect indicated that the triboelectrification between $Mo_6S_3I_6$ and ITO is very impressive, as they are both inorganic materials. Further study of the performance of a TENG constructed with these materials indicated that the maximum open-circuit voltages and the maximum short-circuit currents reached 57 V

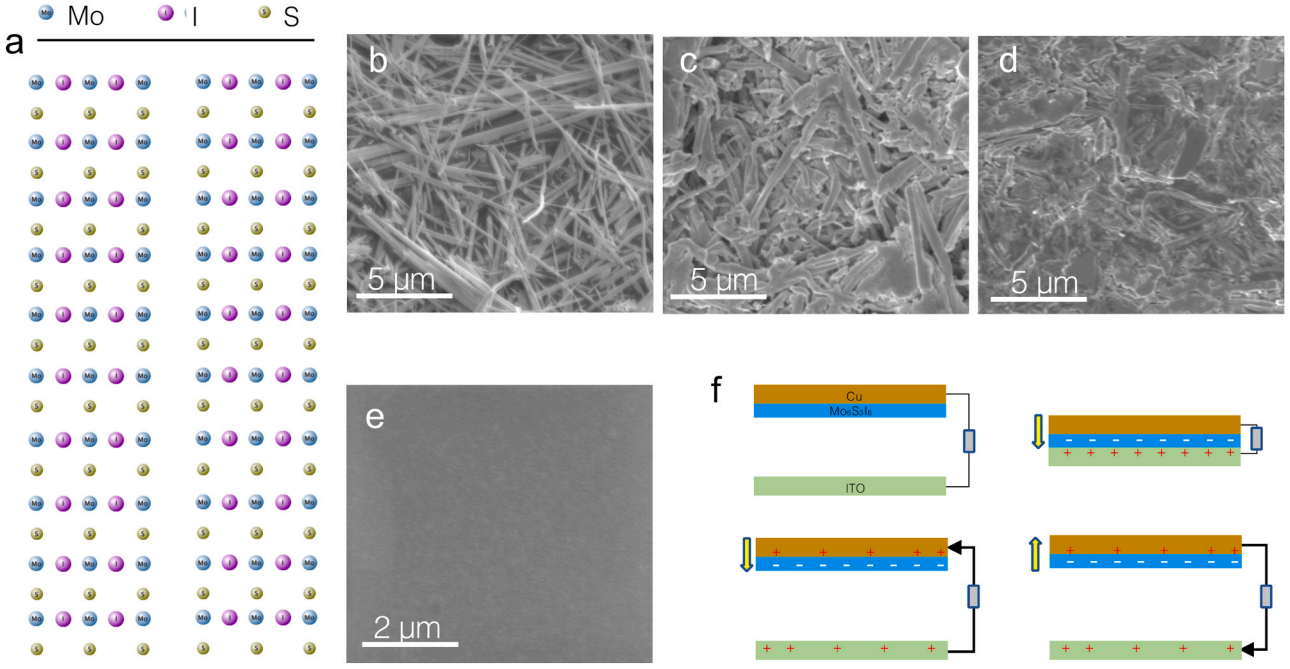


**Fig. 1.** (a) Side view of a bundle of two $Mo_6S_3I_6$ nanowires. (b) SEM image of the $Mo_6S_3I_6$ bundles. (c) SEM image of $Mo_6S_3I_6$ film on copper tape before TENG operation. (d) SEM image of the $Mo_6S_3I_6$ film after several contact separation cycles with ITO. (e) SEM image of ITO film. (f) Schematic drawing of the circuit and operation of TENGs fabricated with $Mo_6S_3I_6$ and ITO.

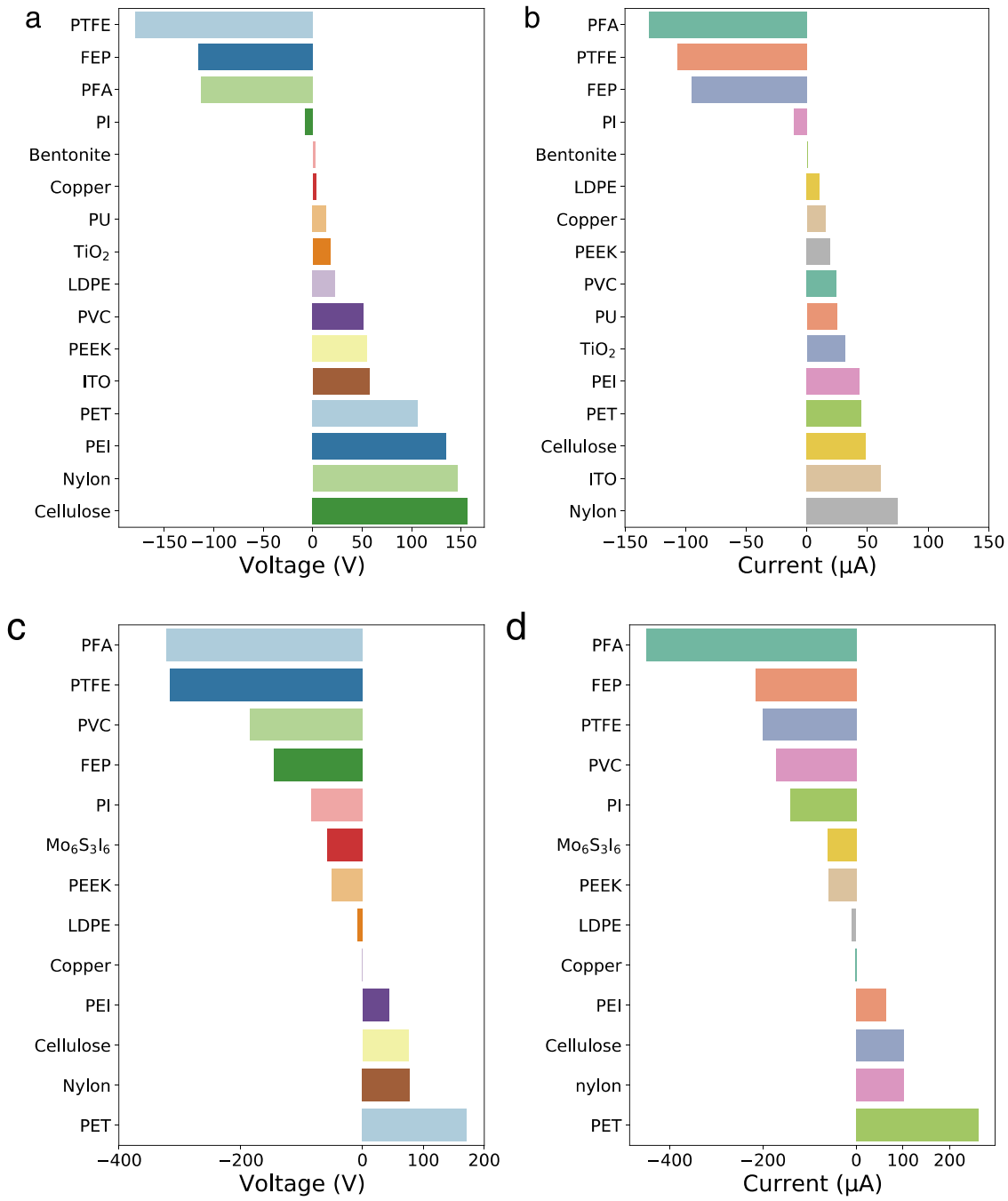


**Fig. 2.** Open-circuit voltages (a, c) and short-circuit currents (b, d) of TENGs fabricated with $Mo_6S_3I_6$ (a, b) or ITO (c, d) and different materials. Bentonite, $TiO_2$ and PU have not been presented in c and d, because no obvious signal has been measured.

and 55 μA, respectively (Fig. S2 in supporting information). The voltage and current at different load resistances are shown in Fig. 3(a), and the results show that the current decreases slowly with increasing resistance. This behavior led to a high output power density of 18.4 W $m^{-2}$ (Fig. 3b) at a load of 50 MΩ, which is approximately one order of magnitude higher than those of other TENGs comprising inorganic materials. [25,26] The output power density of the $Mo_6S_3I_6$/ITO TENG has been found higher than the $Mo_6S_3I_6$/PTFE, $Mo_6S_3I_6$/PFA, $Mo_6S_3I_6$/Nylon, ITO/Nylon TENGs, which is because $Mo_6S_3I_6$/ITO TENG has higher current at high load range above 1 MΩ. The decrease speed of the current for $Mo_6S_3I_6$/ITO TENG is slower than the others, despite the lower current at lower load resistances. Surface discharge maybe one of the reasons for the slower current decrease, while more study is needed to prove assumption.

We have further compared the $Mo_6S_3I_6$/ITO TENG with other TENGs constructed from the triboelectric pairs (Fig. 3c–l) $Mo_6S_3I_6$/PTFE, $Mo_6S_3I_6$/PFA, $Mo_6S_3I_6$/Nylon, ITO/Nylon, and ITO/PFA. The results showed that the other TENGs have higher open-circuit voltages and short-circuit currents (Fig. S3 in supporting information) than the $Mo_6S_3I_6$/ITO TENG. However, the maximum output power densities of these TENGs (Fig. 3d, f, and j) were lower than that of the $Mo_6S_3I_6$/ITO TENG, with the exception of the ITO/PFA TENG (Fig. 3l).

The performance of the $Mo_6S_3I_6$/ITO paired TENG was further tested by using it to charge a 100 μF capacitor (Fig. 4a), and the results indicated that the capacitor was charged up to 1.226 V in 100 s, which corresponds to 75.2 μJ. The stability of the TENG was also tested over 8000 cycles of TENG operation. Fig. 4(b) shows the measurements of the short-circuit current of the TENG at the beginning and end of the 8000

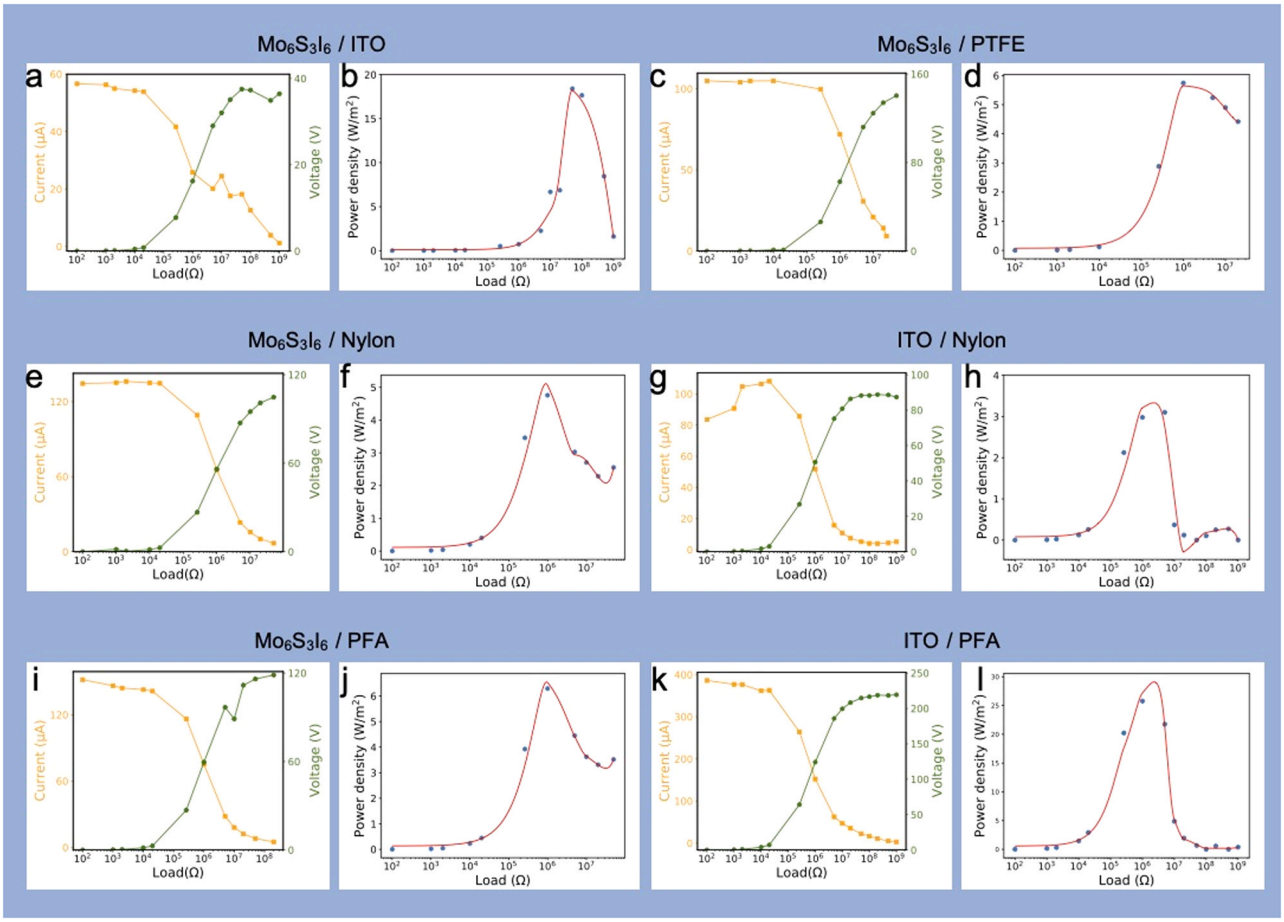


**Fig. 3.** Voltage, current and power density vs. load resistance for TENGs fabricated with the material pairs $Mo_6S_3I_6$/ITO (a, b), $Mo_6S_3I_6$/PTFE (c, d), $Mo_6S_3I_6$/Nylon (e, f), ITO/Nylon (g, h), $Mo_6S_3I_6$/PFA (i, j), and ITO/PFA (k, l). In g, the first two current data points were only measured on the sample that tested on the same day as the other pairs. Lately, we repeat the measurement on another day, the first two points were found normal.

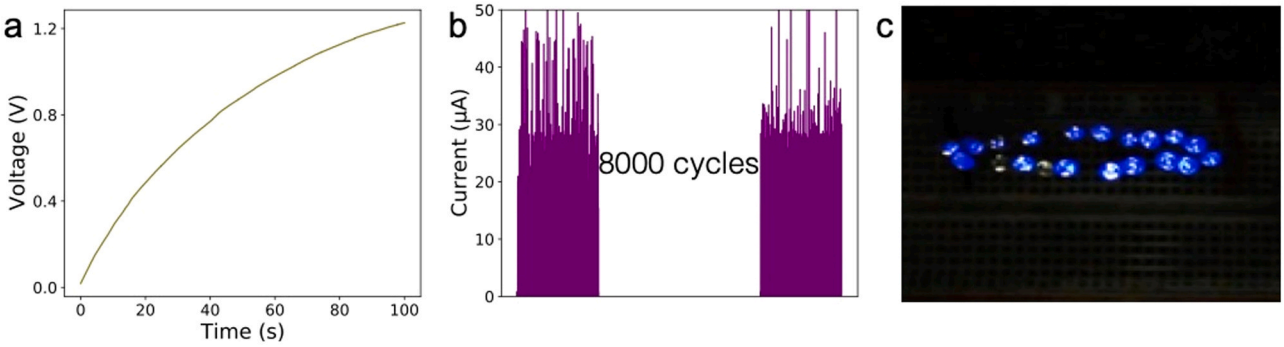


**Fig. 4.** (a) Charge of a 100 μF capacitor with the $Mo_6S_3I_6$/ITO paired TENG. (b) Stability test of the $Mo_6S_3I_6$/ITO TENG for 8000 cycles of operation, showing the short-circuit current. (c) 20 LEDs lit by the $Mo_6S_3I_6$/ITO TENG.

cycles of operation. The signal intensities vary between 30 and 50 μA, which may because of the pins of $Mo_6S_3I_6$ nanowires that created during the contact-separation process. A pin can be created at one contact-separation process and can be eliminated at another process. Such processes could lead to the change of the currents. However, if we look at the behavior at a longer time window, the maximum and the average currents did not change obviously, showing a relevant stability. The performance of the TENG has also been tested by lighting 20 LEDs with the TENG, as shown in Fig. 4(c) (and Video 1 in the Supporting Information).

### 2.3. Mechanisms

The high output power density from the $Mo_6S_3I_6$/ITO paired TENG was considered to result from the unique semiconducting property of the unbundled $Mo_6S_3I_6$ nanowires and the unique chemical composition of ITO. Fig. 1(b) shows that the $Mo_6S_3I_6$ nanowires were originally bundled, but the bundled structure was destroyed after TENG operation. The destroyed bundles are thought to be semiconducting, according to the literature. In this case, $Mo_6S_3I_6$ appears to be a semiconductor with a bandgap of 1.2–1.5 eV and a Fermi level of 4.78 eV. [31] For ITO, the chemical composition comprises tin-doped indium oxide ($In_2O_3$) with a

doping level of approximately 10 at%. [33].

ITO is generally considered a conductive material and is used in electrodes as a metal. However, during the triboelectrification process with $Mo_6S_3I_6$, the semiconductor nature of $In_2O_3$ played a very important role. When uncharged $Mo_6S_3I_6$ contacts uncharged ITO (Fig. 5a), there is a 90% chance that $Mo_6S_3I_6$ will contact the $In_2O_3$. At this moment, there is no electron flow in the ITO, and its conductivity is not activated. Instead, $In_2O_3$ acts as a semiconductor and serves to induce triboelectrification with $Mo_6S_3I_6$. When the charged materials are separated, the positive charges on ITO will be distributed because ITO is conductive. A band diagram showing the triboelectrification process is given in Fig. 5(b). The Fermi level of $In_2O_3$ is approximately 4.3 eV, [34] which is 0.48 eV higher than that of $Mo_6S_3I_6$. When these two materials come into contact, the Fermi levels align at the same point, driving electron flow from $In_2O_3$ to $Mo_6S_3I_6$.

Unlike the charges on the ITO, the charges generated on a polymer such as PTFE will remain at the original location due to the dielectric properties of the polymer (Fig. 5c). A band diagram was also drawn to illustrate the charge transfer between $Mo_6S_3I_6$ and PTFE. For PTFE, which is an organic polymer, the HOMO and LUMO are used to correspond with the valence and conduction bands of semiconductors. There is no Fermi level defined for polymers. However, the chemical potential can be used in the same way as the Fermi level since the Fermi level actually means the chemical potential of the materials. [35] For PTFE, the chemical potential $[(E_{HOMO} + E_{Lumo})/2]$ is at −6.3 eV [36] (Fig. 5d), which is 1.52 eV lower than that of $Mo_6S_3I_6$, and the difference will drive electron transfer from $Mo_6S_3I_6$ to the orbitals of PTFE. The 1.52 eV difference between PTFE and $Mo_6S_3I_6$ is greater than the 0.48 eV difference between $In_2O_3$ and $Mo_6S_3I_6$, which might be the reason for the greater open-circuit voltage for the $Mo_6S_3I_6$/PTFE TENG than for the $Mo_6S_3I_6$/ITO TENG.

## 3. Conclusion

In summary, we reported here a TENG comprising all inorganic materials, with an output power density that is one order of magnitude higher than those of other inorganic-based TENGs. The mechanisms behind the high output have been discussed in detail, and they show that the semiconducting property of $Mo_6S_3I_6$ and the chemical composition of ITO are fundamental. The findings here show the first case in which a TENG with an output power density in the range of tens of watts per square meter was made entirely with inorganic materials. These findings could lead to further development of inorganic TENGs that can be applied under conditions in which organic materials cannot perform well.

## 4. Experimental section

### 4.1. Materials

PTFE was purchased from High-Tech-Flon®. All other plastic films were purchased from McMaster-Carr. Powder samples were purchased from Sigma-Aldrich. $Mo_6S_3I_6$ was obtained from Mo6. The side view of the structure of $Mo_6S_3I_6$ bundles were drawn using MarvinSketch (ChemAxon). $Mo_6S_3I_6$ films were prepared by rubbing the sample on copper tape and manually pressing them with a flat glass. After that, air flow was used to remove unattached residues.

### 4.2. Fabrication of TENGs

All components TENGs were cut to a size of 3 cm × 3 cm and mounted on a linear motor. For powder like materials such as $Mo_6S_3I_6$, bentonite and $TiO_2$, the materials are rubbed on copper tapes with finger and pressed with a flat substrate, and subsequently blow with air to remove loose attached materials. The contact-separation speed of the measurement was set to 0.3 m/s. All experiments were done at a RH of 25% and a temperature of 20 °C.

### 4.3. Measurement

Electrical measurements were performed using a PXI 4071 DMM (National Instruments) with a sampling rate of 100,000/s. The

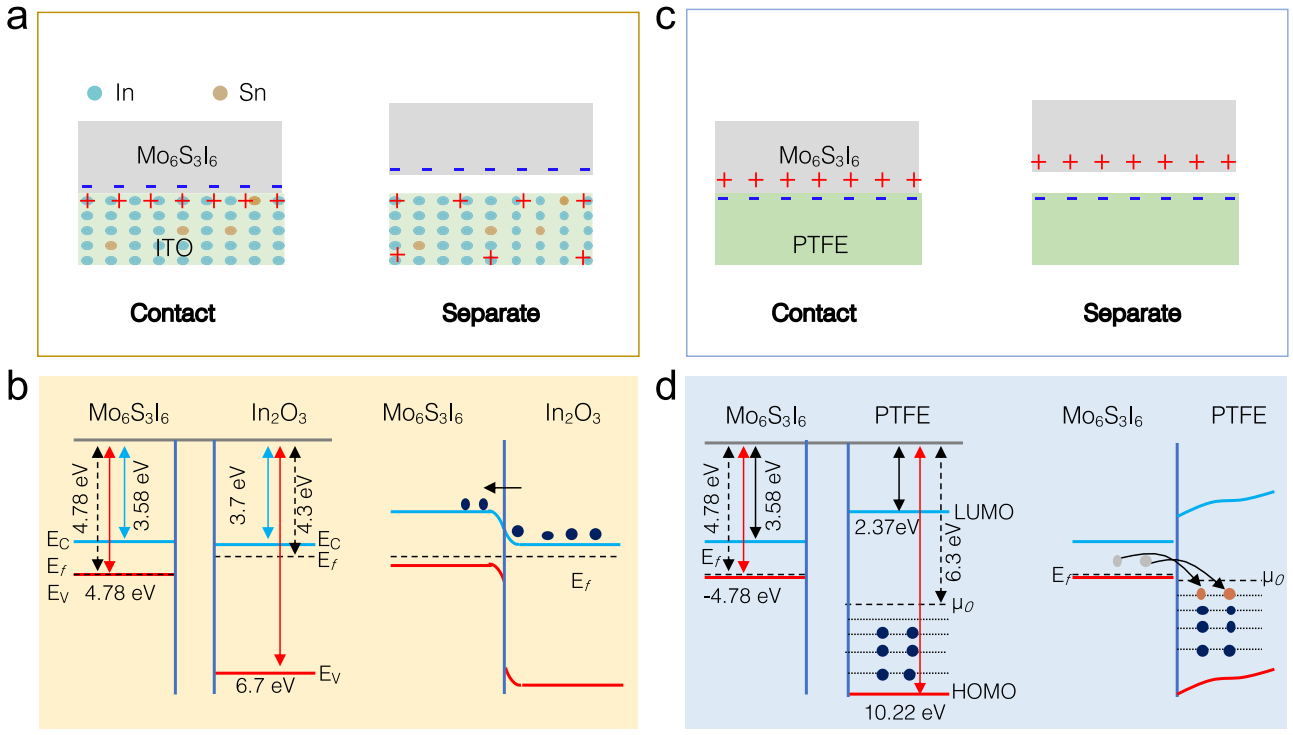


**Fig. 5.** (a) Schematic drawing of triboelectrification between $Mo_6S_3I_6$ and ITO. (b) Band diagram showing charge transfer at the $Mo_6S_3I_6$/ITO interface. (c) Schematic drawing of the triboelectrification between $Mo_6S_3I_6$ and PTFE. (d) Band diagram showing the charge transfer at the $Mo_6S_3I_6$/PTFE interface.

mechanical movement was enabled with a linear motor.

## CRediT authorship contribution statement

**Zhang Renyun:** Conceptualization, Methodology, Experiment, Data Curation, Writing – original draft preparation, Writing – review & editing. **Magnus Hummelgård:** Conceptualization, Measurement system. **Jonas Örtegren, Henrik Andersson, Ya Yang, Zhong-Lin Wang, Håkan Olin:** Writing – review & editing, Discussion. **Martin Olsen**: Writing – review & editing. **Petra Sutar:** Synthesis of $Mo_6I_3S_6$. **Dragan Mihailovic:** Writing – Reviewing and Editing.

## Declaration of Competing Interest

The authors declare that they have no known competing financial interests or personal relationships that could have appeared to influence the work reported in this paper.

## Acknowledgments

This work is financially supported by the European Regional Development Fund, the Energy Agency of Sweden, Stiftelsen Promobilia, Region Västernorrland, Sundsvalls Kommun, Timrå Kommun, and Härnösands Kommun.

## Appendix A. Supporting information

Supplementary data associated with this article can be found in the online version at doi:10.1016/j.nanoen.2021.106363.

## References

[1] R. Zhang, H. Olin, Material Choices for Triboelectric Nanogenerators: A Critical Review, EcoMat. 2 (2020) eom2.12062. https://doi.org/10.1002/eom2.12062.
[2] R. Ccorahua, J. Huaroto, C. Luyo, M. Quintana, E.A. Vela, Enhanced-performance bio-triboelectric nanogenerator based on starch polymer electrolyte obtained by a cleanroom-free processing method, Nano Energy 59 (2019) 610–618, https://doi.org/10.1016/j.nanoen.2019.03.018.
[3] S. Li, J. Nie, Y. Shi, X. Tao, F. Wang, J. Tian, S. Lin, X. Chen, Z.L. Wang, Contributions of different functional groups to contact electrification of polymers, Adv. Mater. 32 (2020), 2001307, https://doi.org/10.1002/adma.202001307.
[4] J. Bian, N. Wang, J. Ma, Y. Jie, J. Zou, X. Cao, Stretchable 3D polymer for simultaneously mechanical energy harvesting and biomimetic force sensing, Nano Energy 47 (2018) 442–450, https://doi.org/10.1016/j.nanoen.2018.03.027.
[5] Z. Wu, W. Ding, Y. Dai, K. Dong, C. Wu, L. Zhang, Z. Lin, J. Cheng, Z.L. Wang, Self-powered multifunctional motion sensor enabled by magnetic-regulated triboelectric nanogenerator, ACS Nano 12 (2018) 5726–5733, https://doi.org/10.1021/acsnano.8b01589.
[6] C. Qiu, F. Wu, C. Lee, M.R. Yuce, Self-powered control interface based on Gray code with hybrid triboelectric and photovoltaics energy harvesting for IoT smart home and access control applications, Nano Energy 70 (2020), 104456, https://doi.org/10.1016/j.nanoen.2020.104456.
[7] C. Zhang, Z.L. Wang, Tribotronics—A new field by coupling triboelectricity and semiconductor, Nano Today 11 (2016) 521–536, https://doi.org/10.1016/j.nantod.2016.07.004.
[8] M. Seol, S. Kim, Y. Cho, K.-E. Byun, H. Kim, J. Kim, S.K. Kim, S.-W. Kim, H.-J. Shin, S. Park, Triboelectric series of 2D layered materials, Adv. Mater. 30 (2018), 1801210, https://doi.org/10.1002/adma.201801210.
[9] J. Du, X. Yang, J. Duan, Y. Wang, Q. Tang, Tailoring all-inorganic cesium lead halide perovskites for robust triboelectric nanogenerators, Nano Energy 70 (2020), 104514, https://doi.org/10.1016/j.nanoen.2020.104514.
[10] G. Zhu, J. Chen, Y. Liu, P. Bai, Y.S. Zhou, Q. Jing, C. Pan, Z.L. Wang, Linear-grating triboelectric generator based on sliding electrification, Nano Lett. 13 (2013) 2282–2289, https://doi.org/10.1021/nl4008985.
[11] Y. Yang, H. Zhang, R. Liu, X. Wen, T.C. Hou, Z.L. Wang, Fully enclosed triboelectric nanogenerators for applications in water and harsh environments, Adv. Energy Mater. 3 (2013) 1563–1568, https://doi.org/10.1002/aenm.201300376.
[12] Y. Xie, S. Wang, L. Lin, Q. Jing, Z.H. Lin, S. Niu, Z. Wu, Z.L. Wang, Rotary triboelectric nanogenerator based on a hybridized mechanism for harvesting wind energy, ACS Nano 7 (2013) 7119–7125, https://doi.org/10.1021/nn402477h.
[13] M. Xu, Y.-C. Wang, S.L. Zhang, W. Ding, J. Cheng, X. He, P. Zhang, Z. Wang, X. Pan, Z.L. Wang, An aeroelastic flutter based triboelectric nanogenerator as a self-powered active wind speed sensor in harsh environment, Extreme Mech. Lett. 15 (2017) 122–129, https://doi.org/10.1016/j.eml.2017.07.005.
[14] Y. Xie, S. Wang, S. Niu, L. Lin, Q. Jing, J. Yang, Z. Wu, Z.L. Wang, Grating-structured freestanding triboelectric-layer nanogenerator for harvesting mechanical energy at 85% total conversion efficiency, Adv. Mater. 26 (2014) 6599–6607, https://doi.org/10.1002/adma.201402428.
[15] C. Yao, A. Hernandez, Y. Yu, Z. Cai, X. Wang, Triboelectric nanogenerators and power-boards from cellulose nanofibrils and recycled materials, Nano Energy 30 (2016) 103–108, https://doi.org/10.1016/j.nanoen.2016.09.036.
[16] F.-R. Fan, Z.-Q. Tian, Z.L. Wang, Flexible triboelectric generator, Nano Energy 1 (2012) 328–334, https://doi.org/10.1016/j.nanoen.2012.01.004.
[17] Y. Wang, Y. Yang, Z.L. Wang, Triboelectric nanogenerators as flexible power sources, Npj Flex. Electron. 1 (2017) 10, https://doi.org/10.1038/s41528-017-0007-8.
[18] L. Lin, Y. Xie, S. Wang, W. Wu, S. Niu, X. Wen, Z.L. Wang, Triboelectric active sensor array for self-powered static and dynamic pressure detection and tactile imaging, ACS Nano 7 (2013) 8266–8274, https://doi.org/10.1021/nn4037514.
[19] B. Meng, X. Cheng, X. Zhang, M. Han, W. Liu, H. Zhang, Single-friction-surface triboelectric generator with human body conduit, Appl. Phys. Lett. 104 (2014), 103904, https://doi.org/10.1063/1.4868130.
[20] Z. Wen, M.-H. Yeh, H. Guo, J. Wang, Y. Zi, W. Xu, J. Deng, L. Zhu, X. Wang, C. Hu, L. Zhu, X. Sun, Z.L. Wang, Self-powered textile for wearable electronics by hybridizing fiber-shaped nanogenerators, solar cells, and supercapacitors, Sci. Adv. 2 (2016), 1600097, https://doi.org/10.1126/sciadv.1600097.
[21] L. Zhang, B. Zhang, J. Chen, L. Jin, W. Deng, J. Tang, H. Zhang, H. Pan, M. Zhu, W. Yang, Z.L. Wang, Lawn structured triboelectric nanogenerators for scavenging sweeping wind energy on rooftops, Adv. Mater. 28 (2016) 1650–1656, https://doi.org/10.1002/adma.201504462.
[22] N. Cui, J. Liu, L. Gu, S. Bai, X. Chen, Y. Qin, Wearable triboelectric generator for powering the portable electronic devices, ACS Appl. Mater. Interfaces 7 (2015) 18225–18230, https://doi.org/10.1021/am5071688.
[23] T. Zhou, C. Zhang, C.B. Han, F.R. Fan, W. Tang, Z.L. Wang, Woven structured triboelectric nanogenerator for wearable devices, ACS Appl. Mater. Interfaces 6 (2014) 14695–14701, https://doi.org/10.1021/am504110u.
[24] H. Zou, L. Guo, H. Xue, Y. Zhang, X. Shen, X. Liu, P. Wang, X. He, G. Dai, P. Jiang, H. Zheng, B. Zhang, C. Xu, Z.L. Wang, Quantifying and understanding the triboelectric series of inorganic non-metallic materials, Nat. Commun. 11 (2020) 1–7, https://doi.org/10.1038/s41467-020-15926-1.
[25] J. Du, J. Duan, X. Yang, Y. Wang, Y. Duan, Q. Tang, Charge boosting and storage by tailoring rhombus all-inorganic perovskite nanoarrays for robust triboelectric nanogenerators, Nano Energy 74 (2020), 104845, https://doi.org/10.1016/j.nanoen.2020.104845.
[26] A. Mahmud, A.A. Khan, S. Islam, P. Voss, D. Ban, Integration of organic/inorganic nanostructured materials in a hybrid nanogenerator enables efficacious energy harvesting via mutual performance enhancement, Nano Energy 58 (2019) 112–120, https://doi.org/10.1016/j.nanoen.2019.01.023.
[27] V. Nicolosi, P.D. Nellist, S. Sanvito, E.C. Cosgriff, S. Krishnamurthy, W.J. Blau, M.L. H. Green, D. Vengust, D. Dvorsek, D. Mihailovic, G. Compagnini, J. Sloan, V. Stolojan, J.D. Carey, S.J. Pennycook, J.N. Coleman, Observation of van der Waals driven self-assembly of MoSI nanowires into a low-symmetry structure using aberration-corrected electron microscopy, Adv. Mater. 19 (2007) 543–547, https://doi.org/10.1002/adma.200601867.
[28] S. Chae, S. Oh, K.H. Choi, J. Jeon, Z. Liu, C. Wang, C. Lim, X. Dong, C. Woo, G. Asghar, J. Chang, M. Nurunnabi, J. Kang, S.Y. Song, H.K. Yu, J.-Y. Choi, Aqueous dispersion of one-dimensional van der waals material Mo 6 S 3 I 6 with the charge type of the hydrophobic dispersant tail, ACS Appl. Bio Mater. 3 (2020) 3992–3998, https://doi.org/10.1021/acsabm.0c00541.
[29] D. Vrbanic, S. Pejovnik, D. Mihailovic, Z. Kutnjak, Electrical conductivity of Mo6S3I6 and Mo6S4.5I4.5 nanowires, J. Eur. Ceram. Soc. 27 (2007) 975–977, https://doi.org/10.1016/j.jeurceramsoc.2006.04.125.
[30] I. Vilfan, D. Mihailovic, Nonlinear elastic and electronic properties of Mo6S3I6, Phys. Rev. B 74 (2006), 235411, https://doi.org/10.1103/PhysRevB.74.235411.
[31] M. Strojnik, A. Omerzu, A. Majkić, P.M. Mihailovic, J. Lukan, G. Bavdek, G. Bratina, D. Cvetko, P. Topolovsek, D. Mihailovic, Ionization energy and energy gap structure of MoSI molecular wires: Kelvin probe, ultraviolet photoelectron spectroscopy, and cyclic voltammetry measurements, Langmuir 27 (2011) 4296–4299, https://doi.org/10.1021/la1050767.
[32] R. Zhang, M. Hummelgård, D. Dvorsek, D. Mihailovic, H. Olin, Mo6S3I6-Au composites: synthesis, conductance, and applications, J. Colloid Interface Sci. 348 (2010) 299–302, https://doi.org/10.1016/j.jcis.2010.04.047.
[33] A. Chen, K. Zhu, H. Zhong, Q. Shao, G. Ge, A new investigation of oxygen flow influence on ITO thin films by magnetron sputtering, Sol. Energy Mater. Sol. Cells 120 (2014) 157–162, https://doi.org/10.1016/j.solmat.2013.08.036.
[34] O. Lang, C. Pettenkofer, J.F. Sánchez-Royo, A. Segura, A. Klein, W. Jaegermann, Thin film growth and band lineup of $In_2O_3$ on the layered semiconductor InSe, J. Appl. Phys. 86 (1999) 5687–5691, https://doi.org/10.1063/1.371579.
[35] M.K. Brachman, Fermi level, chemical potential, and Gibbs free energy, 1152–1152, J. Chem. Phys. 22 (1954), https://doi.org/10.1063/1.1740312.
[36] W. Wang, T. Takada, Y. Tanaka, S. Li, Space charge mechanism of polyethylene and polytetrafluoroethylene by electrode/dielectrics interface study using quantum chemical method, IEEE Trans. Dielectr. Electr. Insul. 24 (2017) 2599–2606, https://doi.org/10.1109/TDEI.2017.006417.